J Mater Sci (2010) 45:3007–3015
DOI 10.1007/s10853-010-4302-1

The influence of Ca on the corrosion behavior of new die cast Mg–Al-based alloys for elevated temperature applications

E. Dabah · G. Ben-Hamu · V. Lisitsyn · D. Eliezer · K. S. Shin

Received: 8 October 2009 / Accepted: 5 February 2010 / Published online: 23 February 2010

Abstract In this study, the corrosion behavior of Mg–5Al alloys with different quantities of calcium was investigated by DC and AC polarization and immersion tests. The alloys' microstructure was investigated by optical microscopy and SEM with EDS. It was found that increasing the Ca content from 0.9 to 1.8 wt% improves the corrosion resistance of the alloy; the corrosion resistance of the alloy with 1.8 wt% Ca equals that of the base Mg–5Al alloy. Ca addition causes a reduction of the average grain size, which increases corrosion resistance as the precipitates located at grain boundaries are more continuous and act as a barrier to the advance of corrosion. The precipitates located at grain boundaries contain Al and Ca and are much less cathodic than the β phase, thus making the microgalvanic effect in the specimen less effective.

Introduction

The concept of weight reduction recently adopted by the transportation industry has made Mg alloys a very interesting choice for many structural applications [1]. The potential opportunities for the use of Mg alloys in motor vehicle components are numerous. This is not solely a result of Mg's relatively low density, which can reduce vehicle weight, but is also a result of its good damping characteristic, dimensional stability, machinability, and low casting cost. As a consequence, these light alloys have a promising future. However, the high susceptibility of Mg alloys to corrosion limits their application in automotive and aerospace industries [2].

The majority of the increase in Mg research has been in the area of die cast components and some semisolid formed components [3]. The corrosion behavior of Mg alloys has been extensively studied for various cast alloys (e.g., AM50 and AZ91) [4–12]. However, the application temperature of these alloys is generally limited to around 100 °C. At higher temperatures a rapid degradation of mechanical properties was observed because of the low stability of the $Mg_{17}Al_{12}$ phase [13–18]. For elevated temperature applications, a series of alloying elements are applied, e.g., Ca, Sr, and rare earth (RE) elements, for formation of thermally stable intermetallic phases [19, 20].

In this study, Ca, which is known to produce thermally stable precipitates such as Al_2Ca and Mg_2Ca, was chosen as the alloying element as it is more economical and lighter than the RE elements. It was found by Shin et al. [16] that Ca addition increases the mechanical properties of Mg–5Al alloy at elevated temperatures (150–200 °C). However, there is a lack of knowledge about the influence of Ca addition on the corrosion behavior of these alloys.

The objective of this work is to study the effect of Ca addition on the microstructure of the selected alloy and its influence on the corrosion behavior.

Experimental

Die cast process

In this study, all test specimens of the Mg–Al–Ca alloys were die cast on a 320 ton high pressure die casting

E. Dabah · G. Ben-Hamu · V. Lisitsyn · D. Eliezer (✉)
Department of Materials Engineering, Ben-Gurion University of the Negev, Beer-Sheva 84105, Israel
e-mail: deliezer@bgu.ac.il

K. S. Shin
Magnesium Technology Innovation Center, School of Materials Science and Engineering, Seoul National University, 599 Gwanangno, Gwanak-gu, Seoul 151-744, Korea

Table 1 Chemical composition of the die cast specimens

Alloy designation	Content (wt%)		
	Al	Ca	Mg
Mg–5Al	4.9	–	Bal.
Mg–5Al–1.0Ca	4.9	0.9	Bal.
Mg–5Al–1.5Ca	4.9	1.4	Bal.
Mg–5Al–2.0Ca	4.9	1.8	Bal.

machine (HPDC) as 80 × 100 mm plates. The plates are composed of two 8 × 5 plates with thicknesses of 5 and 3 mm. The chemical composition of the alloys is summarized in Table 1.

Microstructure analysis

For optical microscopy and SEM observations the samples were polished up to 1 μm using diamond polishing compound and nonaqueous lubricants, etched using a solution of 10 mL acetic acid, 4.2 g picric acid, 10 mL H_2O, and 70 mL ethanol, and ultrasonically cleaned in acetone and ethanol for 1 min. The microstructure was observed using a Nikon Epishot microscope and by SEM microscope type JEOL JSM 6500F equipped with EDS.

For metallographic observations, cross-section specimens were made and photographs were taken both from the surface and as far as 1 mm from the surface (bulk).

The corroded surfaces, after removal of the corrosion products, were observed after ½, 1, and 3 h using SEM.

Corrosion and electrochemical tests

The corrosion behavior of the Mg–5Al–*x*Ca alloys was investigated using potentio-dynamic polarization (PD) measurements, electrochemical impedance spectroscopy (EIS), and immersion tests. All the corrosion tests were performed in 3.5% NaCl water solution saturated with $Mg(OH)_2$ at pH 10.5, at which Mg can be covered with a more or less protective oxide or hydroxide layer that checks the dissolution reaction [21].

The immersion test specimens were polished up to a 6 μm SiC (1200 grid) and were cleaned ultrasonically in acetone and alcohol. The immersion test was carried out at room temperature for 72 h. Final cleaning of the specimens from the corrosion products was conducted by immersing them in a solution of 200 g/L CrO_3 and 10 g/L silver nitrate in distilled water. The weight loss of the specimens was obtained with a precision of 0.01 mg.

The potentio-dynamic test system basically consists of the corrosion cell with a luggin capillary and electrolyte bridge to the cell for a reference electrode. A saturated calomel electrode (SCE) was used as reference electrode. The test specimens were polished using 1-μm diamond polishing compound to reduce the surface roughness and preserve the "skin" layer of the die cast specimen. The potentio-dynamic polarization tests were conducted using a scan rate of 5 mV/s and scan range from −2000 to 0 mV, with the electrode activated by cathodic current prior to anodic polarization. All polarization curves were obtained using the corrosion measurement system consisting of a Versastat-Potentiostat/Galvanostat with floating option, EG&G Princeton electrochemical cell (KO235 flat type), EG&G Princeton potentiostat (Model 263 Versastat F), and a personal computer. The corrosion rate was calculated by Tafel extrapolation.

The impedance measurements were carried out using a PARSTAT 2263 frequency response analyzer coupled with the potentiostat. All the experiments were controlled by a PC, which was also used for the acquisition, storage, and plotting of data. The scanned frequency ranged from 6 MHz to 100 kHz and the perturbation amplitude was 5 mV (it was observed that a variation in the amplitude did not change the frequency response of the electrode/electrolyte interface). The impedance measurements were performed at open circuit potential (Eocp). A partial data fitting made with the Boukamp circuit equivalent software [21] for the charge-transfer process produced the Rp (polarization resistance) and C_{dl} (double-layer capacitance) values.

Scanning Kelvin probe force microscopy (SKPFM)

The local potential difference on the surface resulting from different compositions of second phase particles in the matrix was investigated using SKPFM technique. The topographic and potential maps of the samples were recorded using a Nanoscope III Multimode SPM equipped with an Extender TM Electronic Module. The scanning Kelvin probe force microscopy characterization was carried out in air at room temperature with 20–40% relative humidity. The scan height in the lift mode was 100 nm. The topography and potential were obtained with a pixel density of 256 × 256 and a scan frequency of 0.1 Hz. For all measurements, commercially available *n*+-silicon tips coated with $PtIr_5$ were used. Prior to each experiment, the tip was checked with a potential measurement on a reference sample, consisting of aluminum partially covered with a thin gold layer. The samples, after polishing up to 1 μm and ultrasonic cleaning, were taken immediately for Volta potential measurements. The phases present in the alloys were identified by SEM microscope equipped with EDS.

Results

Microstructure

The optical micrographs in Figs. 1, 2, and 3 present the morphology of the Mg–Al alloys with different Ca contents. It can be seen in Fig. 4 that the grain size decreases with the addition of Ca. Moreover, the grain size in the area about 0.75–1 mm from the surface (bulk) is larger than that at the surface of the specimen. The 3-mm-thick specimens have a smaller grain size than the 5-mm-thick specimens due to different cooling rates in the die cast process [22]. As the Ca content increases, the influence of the die geometry on grain size decreases as the average grain size difference decreases with additional Ca content.

The SEM micrograph (Fig. 5) and EDS results show that the Mg–5Al–2.0Ca alloy microstructure consists of α-Mg matrix and an Al/Ca rich phase located at grain boundaries.

Scanning Kelvin probe force microscopy

The SKPFM results (Fig. 6) show that the phase located at the grain boundaries is brighter than the matrix background, thus suggesting that this phase is noble relative to the Mg matrix. The measurements on the surface of a Mg–5%Al–2.0%Ca alloy showed a positive potential difference (59 ± 6 mV) that is similar to that previously found by Apachitei et al. (62 ± 5 mV) [23] between the Al_2Ca phase and the Mg matrix. This positive potential difference suggests that this phase is acting as an active cathode. This potential difference is lower than that of the β phase (140–200 mV) previously identified [23].

Corrosion and electrochemical tests

Immersion test

Immersion test—the corrosion rates calculated from the 72-h immersion test in a 3.5% NaCl water solution saturated with $Mg(OH)_2$ are shown in Fig. 7. An increase in corrosion rate with the addition of up to 1 wt% Ca and a decrease in corrosion rate with further addition of Ca are noted. Moreover, the 3-mm-thick specimens exhibit better corrosion resistance than that of the 5-mm-thick specimens.

Potentio-dynamic polarization test

The potentio-dynamic polarization test is a very powerful tool for estimating the kinetics of the corrosion process. The results of the corrosion current after 4-h immersion (Table 2), acquired from Fig. 8b, d, are proportional to the corrosion rate, showing the same tendency as the results acquired from the immersion test as can be seen in Fig. 9. From an observation of the results in Fig. 8a, c at $t = 0$ h, it can be seen that the Mg–5Al–1.0Ca alloy exhibits the greatest corrosion potential. After 4-h immersion, the corrosion potential increases with the addition of Ca. At all immersion times the Mg–5Al–1.0Ca alloy exhibits the highest cathodic activity.

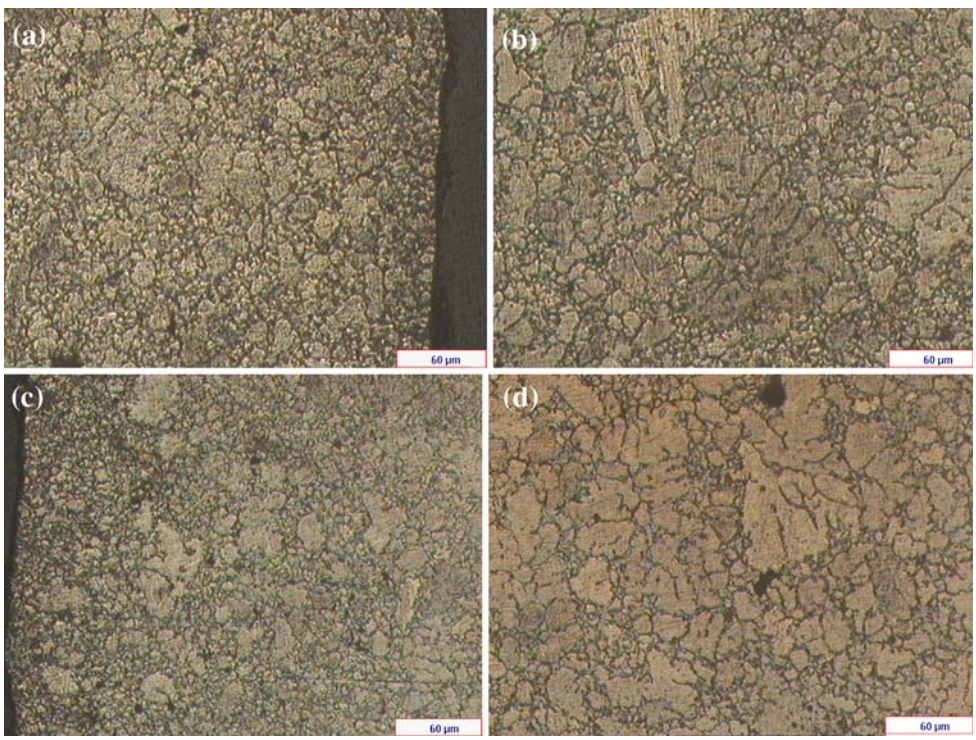

Fig. 1 Optical micrographs of Mg–5Al–1.0Ca: **a** 3 mm surface, **b** 3 mm bulk, **c** 5 mm surface, **d** 5 mm bulk

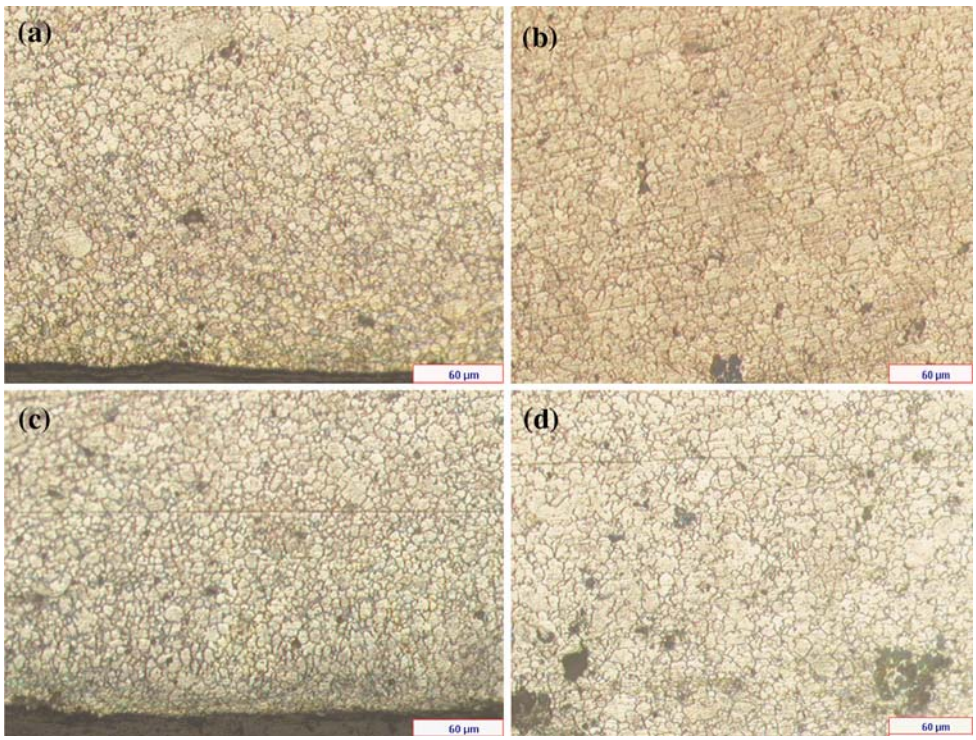

Fig. 2 Optical micrographs of Mg–5Al–1.5Ca: **a** 3 mm surface, **b** 3 mm bulk, **c** 5 mm surface, **d** 5 mm bulk

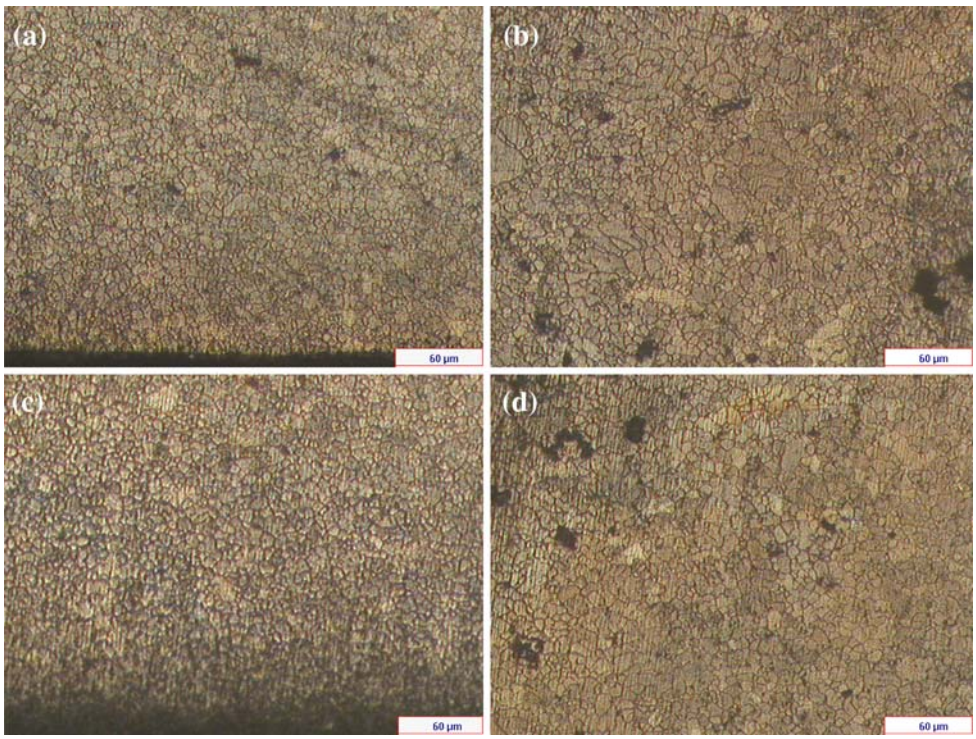

Fig. 3 Optical micrographs of Mg–5Al–1.8Ca: **a** 3 mm surface, **b** 3 mm bulk, **c** 5 mm surface, **d** 5 mm bulk

Electrochemical impedance spectroscopy

Electrochemical impedance spectroscopy (EIS) is a useful technique in the study of corrosion. The simple electrochemical system consists of a double-layer capacitance (C_{dl}), solution resistance (R_s), and charge-transfer resistance (R_p). The characteristic parameters of these elements' values are obtained directly by fitting the experimental impedance curves using Boukamp software. These electrochemical parameters are listed in Table 3. The EIS results of Mg–5Al–*x*Ca alloy are shown in Fig. 10 as both Nyquist and Bode plots. The Nyquist plot (Fig. 10a) shows

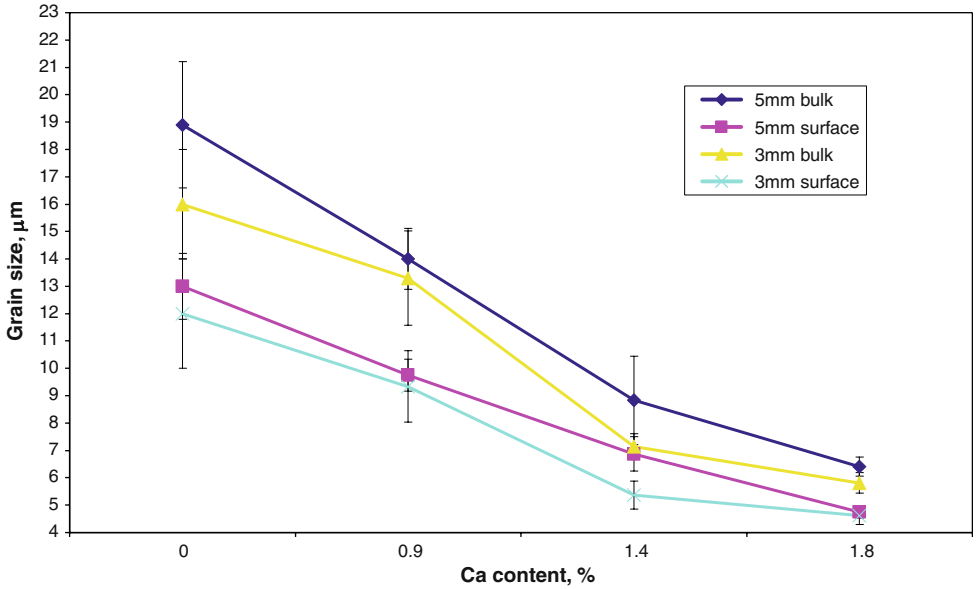

Fig. 4 Grain size dependence on Ca content

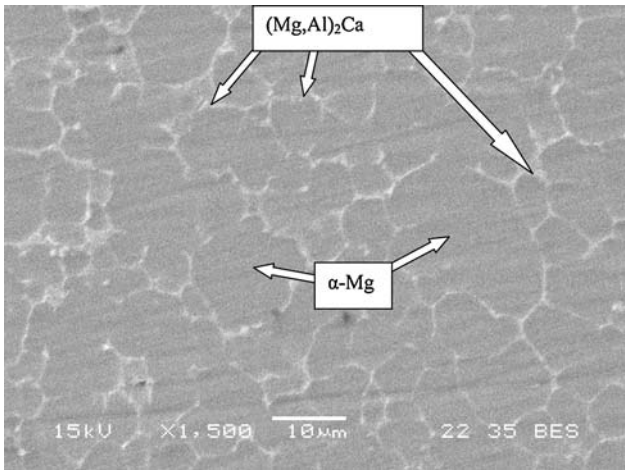

Fig. 5 SEM micrographs of Mg–5Al–2.0Ca surface

that all the curves have a single capacitive loop at all frequencies. The diameter of the capacitive semicircle is closely related to the corrosion rate. The EIS spectra are similar except in diameter, showing that the corrosion mechanism is the same, differing only in rate. The diameters of the capacitive loops of Mg–5Al and alloys with 2.0 wt% Ca are almost the same. As expected, a lesser diameter is obtained with 1.0 wt% Ca addition, which indicates that the corrosion resistance of Mg–5Al–1.0Ca is reduced by addition of 1.0 wt% Ca. The corrosion rate is inversely related to R_p—the greater the value of R_p, the greater the corrosion resistance (smaller corrosion rate). Greater R_p value obtains with addition of 2.0 wt% Ca; the lower value with 1.0 wt% Ca addition reflects the alloy behavior during corrosion.

In general, the C_{dl} value for the magnesium alloys is low and is attributed to the formation of a relatively thick and compact protective film on the metal surface [24, 25]. In this study, it is also seen that an increase in R_p is not accomplished by the reduction of C_{dl}; however, the C_{dl} values are increased with an increase in R_p values. A similar observation has been made, by Srinivasan et al. [26] with the addition of Si to AZ91 alloy. These results indicate that the Mg–5Al–(1.0–2.0)Ca alloys cannot form an effective protective film in a chloride environment. The Bode plot in Fig. 10b shows the low frequency impedance values for different alloys. A greater impedance value is noticed with addition of 2.0 wt% Ca. Lower impedance value is noticed with 1.0 wt% Ca addition, which is in line with the immersion and polarization test results.

Corrosion morphology

The corrosion morphology of specimens immersed in 3.5% NaCl water solution saturated with $Mg(OH)_2$, after 30, 60, and 180 min is shown in Figs. 11, 12, and 13, respectively. It can clearly be seen that pitting corrosion occurs. The corrosion process is initiated at the interfaces between the α-Mg and the Al-rich phases due to galvanic coupling between these phases. As the corrosion process precedes, α-Mg grains dissolved, thus making the Al-rich phases flake away, forming large corrosion pits.

Discussion

The differences in corrosion resistance with the addition of up to 1.8% Ca are related mostly to the different microstructure and distribution of the β and Al_2Ca phases. As the Ca content increases, the grain size decreases and the volume fraction of the second phases increases (more

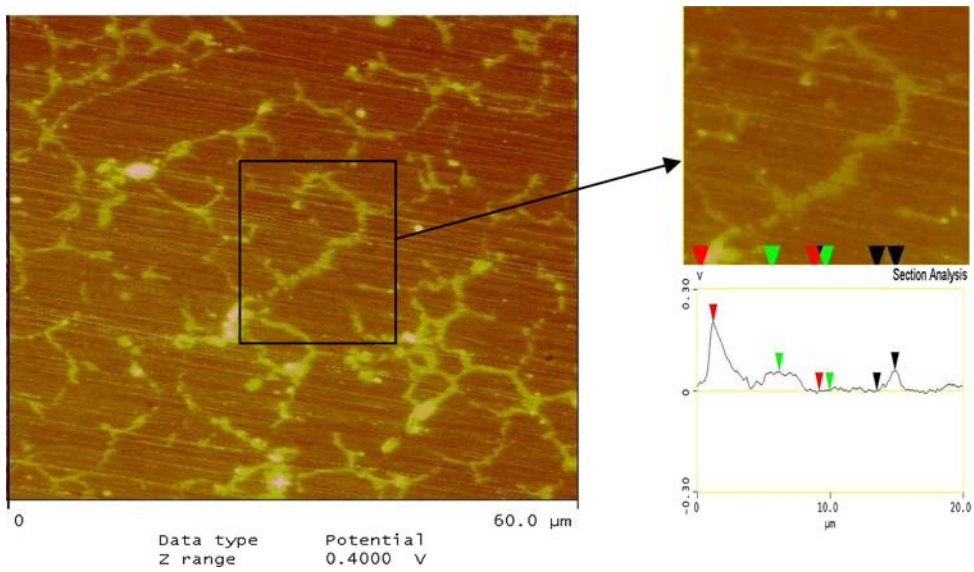

Fig. 6 SKPFM measurement of Mg–5Al–2.0Ca

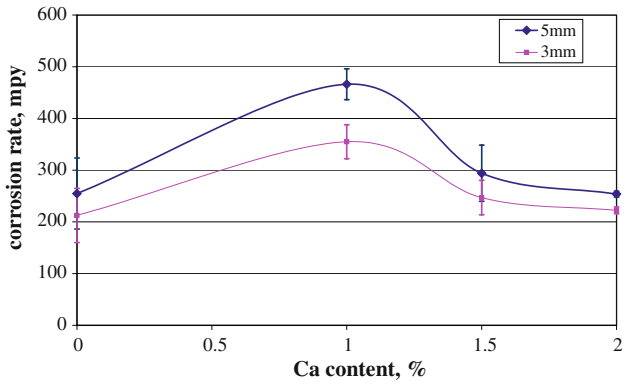

Fig. 7 Results of 72-h immersion test

Table 2 E_{corr} and I_{corr} values of Mg–5Al–XCa alloys after 4 h immersion

	Alloy i_{corr} (µA/cm^2) 5 mm/3 mm	E_{corr} (V) 5 mm/3 mm
Mg–5%Al	2330/1920	−1.573/−1.557
Mg–5%Al–1.0%Ca	3820/2850	−1.540/−1.533
Mg–5%Al–1.5%Ca	3050/2470	−1.512/−1.486
Mg–5%Al–2.0%Ca	2310/2520	−1.486/−1.501

precipitates are distributed along the grain boundaries). The large quantity of second phases at the surface creates more microgalvanic sites. Therefore, addition of Ca in Mg–5%Al alloy increases the corrosion rate. However, when increasing the Ca content up to 1.8 wt%, the distribution of the second phase near the surface area becomes more continuous, and the presence of Ca induces the formation of the less cathodic Al_2Ca phase on the expanse of the more cathodic β phase. In addition, due to the high Al content in the grain boundaries this area acts as a corrosion barrier [27, 28].

Even though fine grains microstructures induce more area to be covered by second phases, the second phase distribution following die cast process is denser at the near surface areas.

It was found that the high temperature mechanical properties of the Mg–5%Al alloys were significantly improved by addition of Ca [29]. From the corrosion study it was found that addition of up to 1.4 wt% Ca increases the corrosion rate of the Mg–5%Al alloys. However, the behavior of the alloy containing 1.8 wt% Ca (Mg–5%Al–2%Ca) was similar to the alloys containing no Ca (Mg–5%Al), thus implying better mechanical properties with the same corrosion resistance. This can be very useful for industrial applications, as the Mg–5%Al–2%Ca alloy exhibits the desired combination of high thermal stability and high corrosion resistance.

Conclusions

1. A refined microstructure has a significant effect on the corrosion resistance of the alloy. Smaller grain size means an increased grain boundaries area, which prevents the second phases to be spread continuously along grain boundaries, thus neglecting its role as a barrier for corrosion advance. However, increasing the content of the refiner element increases the volume fraction of the second phases thus creating a continuous phase along grain boundaries.
2. The microstructure of the die cast Mg–5Al–*x*Ca alloys depends on cooling rate and Ca content. Faster cooling rate causes an increase in nucleation rate, thus

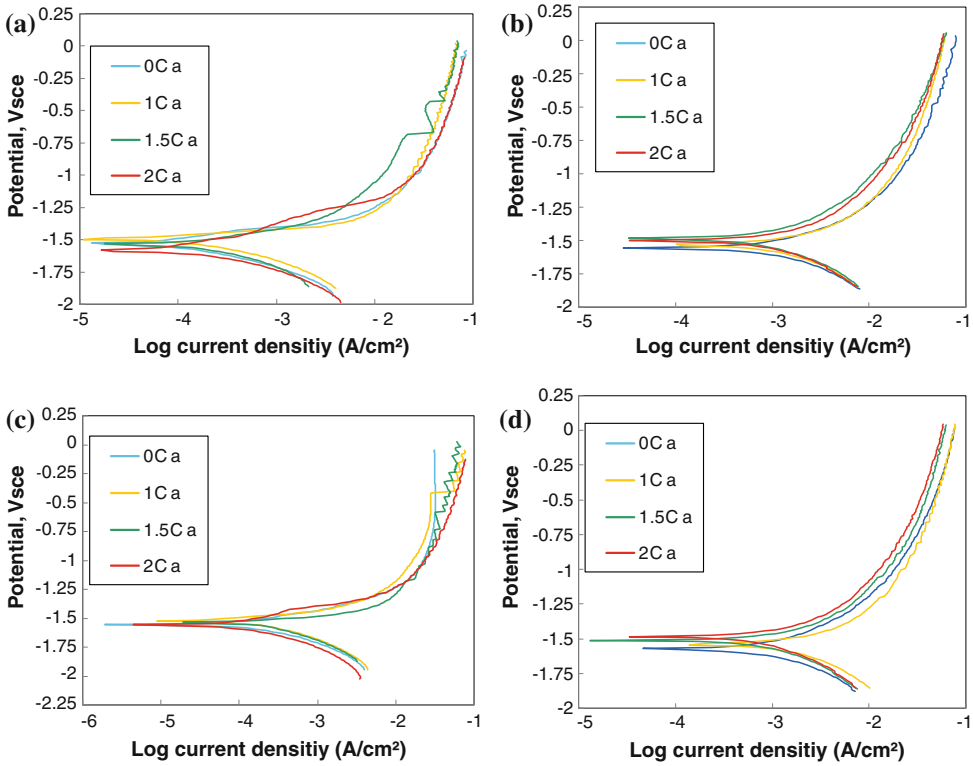

Fig. 8 PD polarization test curves **a** 3 mm thickness at $t = 0$ h, **b** 3 mm thickness at $t = 4$ h, **c** 5 mm thickness at $t = 0$ h, **d** 5 mm thickness at $t = 4$ h

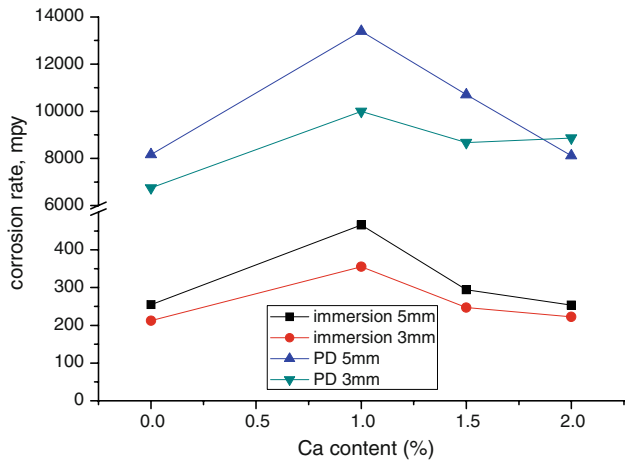

Fig. 9 Comparison of corrosion rates from immersion and PD tests

Table 3 Corrosion parameters obtained from EIS measurement for ZSM6*X*0 alloys

Alloy	|Z|, (Ω cm^2)	R_p, (Ω cm^2)	C_{dl}, (μF)
Mg–5Al	363	398	16.4
Mg–5Al–1.0Ca	167	168	110.4
Mg–5Al–1.5Ca	233	234	54.7
Mg–5Al–2.0Ca	251	257	28.6

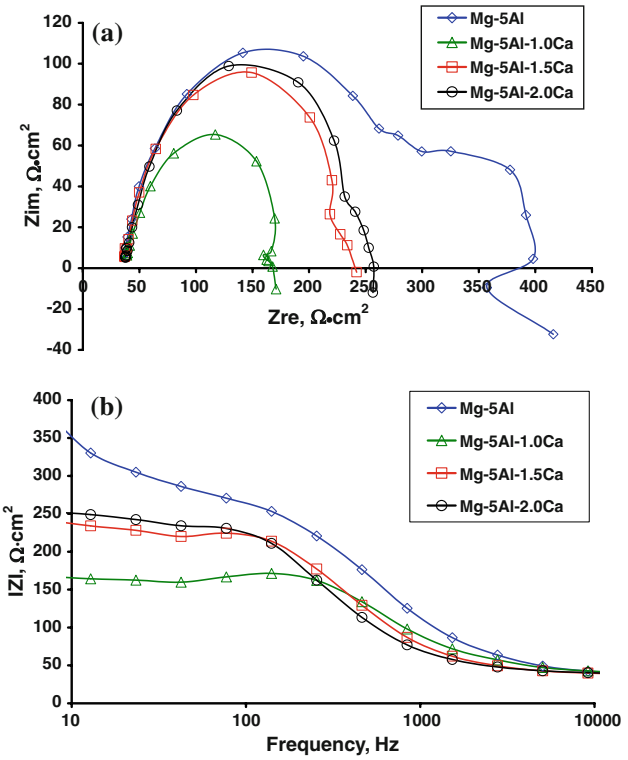

Fig. 10 Electrochemical impedance spectroscopy measurements of Mg–5Al–XCa alloys. **a** Nyquist plot and **b** Bode plot

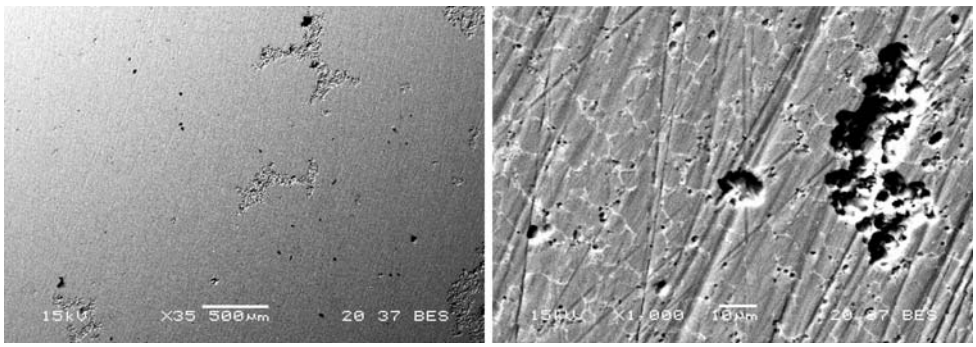

Fig. 11 Corrosion morphology after 30 min

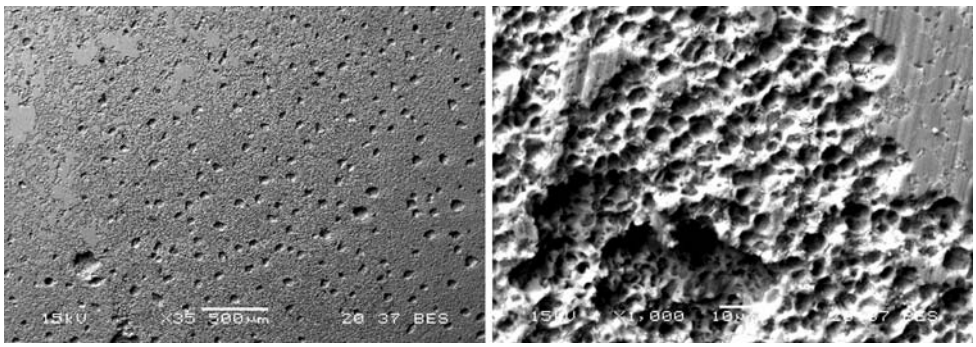

Fig. 12 Corrosion morphology after 1 h

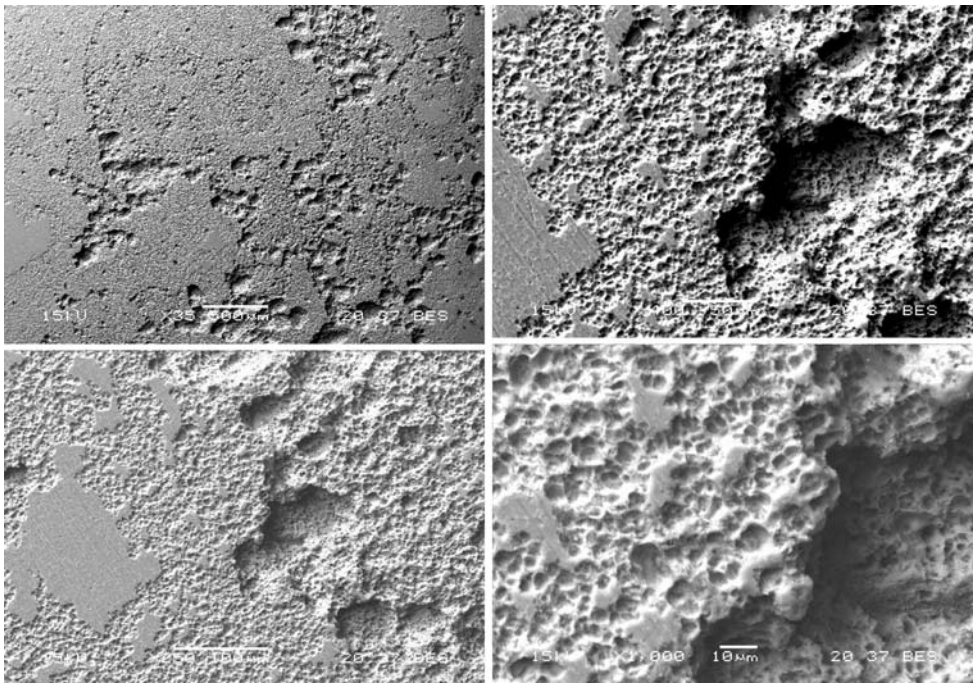

Fig. 13 Corrosion morphology after 3 h

decreasing grain size. Increase of the Ca content suppresses grain growth by the precipitation of second phase which inhabits the migration of grain boundaries.

3. The potential difference between Al_2Ca phase precipitates and the Mg matrix is lower compared with that of $Mg_{17}Al_{12}$ phase; thus Al_2Ca precipitate formation makes the galvanic effect less intensive.
4. Ca alloying up to 0.9 wt% increases the corrosion rate relative to the base Mg–5Al alloy due to the appearance of new electrochemical sites of Al_2Ca phase. Further increase of Ca content up to 1.8 wt% improves corrosion resistance due to the replacement of the $Mg_{17}Al_{12}$ phase with a less cathodic Al_2Ca phase.
5. The corrosion resistance of Mg–5Al–2.0Ca alloy is similar to that of the Mg–5Al alloy, but has improved

mechanical properties at elevated temperatures, thus making this alloy applicable for elevated temperature applications.

References

1. Eliezer D, Alves H (2002) In: Kuts M (ed) Handbook of materials selection. Wiley, New York, p 267
2. Song GL, Atrens A (1999) Adv Eng Mater 1:11
3. Yim CD, Shin KS (2003) Mater Trans 44(4):558
4. Avedesian M, Baker H (1998) ASM international, Materials Park
5. Eliezer D, Uzan P, Aghion E (2003) Mater Sci Forum 419–422:857
6. Mathieu S, Rapin C, Steinmetz J, Steinmetz P (2003) Corros Sci 45:2741
7. Raman RKS (2004) Metall Mater Trans A 35:2525
8. Ko YJ, Yim CD, Lim JD, Shin KS (2003) Mater Sci Forum 419–422:851
9. Song G, Bowles AL, St John DH (2004) Mater Sci Eng A 366:74
10. Aghion E, Lulu EN (2009) J Mater Sci 44(16):4279. doi:10.1007/s10853-009-3634-1
11. Aghion E, Gueta Y, Moscovitch N et al (2008) J Mater Sci 43(14):4870. doi:10.1007/s10853-008-2708-9
12. Aal AA (2008) J Mater Sci 43(8):2947. doi:10.1007/s10853-007-1796-2
13. Luo AA (2003) Mater Sci Forum 419–422:57
14. Pekguleryuz MO (2004) Magnes Technol 2004:281
15. Mordike BL (2002) Mater Sci Eng A 324:103
16. Cho WC, Jung HC, Shin KS (2005) Proceedings of the 1st Asian symposium on magnesium alloys. Jeju, Korea, 11–14 Oct 2005
17. Moreno IP, Nandy TK, Jones JW, Allison JE, Pollock TM (2003) Scripta Mater 48:1029
18. Wang RM, Eliezer A, Gutman E (2003) Mater Sci Eng A 344:279
19. Liu N, Wang JL, Wu YM et al (2008) J Mater Sci 43(8):2550. doi:10.1007/s10853-008-2447-y
20. Buha J (2008) J Mater Sci 43(4):1220. doi:10.1007/s10853-007-2250-1
21. Ben-Hamu G, Eliezer D, Shin KS (2007) Mater Sci Eng A 447:35
22. Aghion E, Moscovitch N, Arnon A (2007) Mater Sci Eng A 447:341
23. Apachitei I, Fratila-Apachitei LE, Duszczyk J (2007) Scripta Mater 57:1012
24. Aung NN, Zhu W (2002) J Appl Electrochem 32:1397
25. Ben-Hamu G, Eliezer D, Shin KS (2007) Mater Sci Eng A 447(1–2):35
26. Srinivasan A, Ningshen S, Kamachi Mudali U, Pillai UTS, Pai BC (2007) Intermetallics 15:1511
27. Ben-Hamu G, Eliezer A, Gutman EM (2006) Electrochim Acta 52(1):304
28. Song G, Atrens A, Dargusch M (1999) Corros Sci 41:249
29. Cho WC, Chul HC, Shin KS (2005) Proceedings of the 1st Asian symposium on magnesium alloys. Jeju, Korea, 11–14 Oct 2005